Astronomical and Astrophysical Transactions (*AApTr*), 2024, Vol. 34, Issue 2, pp. 111–120,
ISSN 1055-6796, Photocopying permitted by license only, ©Cambridge Scientific Publishers

DR21(OH) sub-cores: inferring the evolutionary status with the PRESTALINE tool

O.V. Kochina[1,*], D.S. Wiebe[1,2]

[1] *Institute of Astronomy, Russian Academy of Sciences, 119017, 48 Pyatnitskaya Str., Moscow, Russia*
[2] *Lebedev Physical Institute, Samara Branch, 443011, 221 Novo-Sadovaya Str., Samara, Russia*

Received 19 October, 2023

In the presented work we demonstrate results of the chemical modelling of two sub-cores in a well-known region of massive star-formation DR21(OH): MM1a and MM1b. These sub-cores, even though situated in close proximity to each other, exhibit distinguishable differences in their observed spectra. Calculations of the chemical evolution and synthetic spectra for these regions, performed using the PRESTALINE (PRESTA + RADEX) tool, allowed us to trace and explain the origin of these features.

Keywords: Star formation, ISM, astrochemistry, synthetic spectra

1 Introduction

DR21(OH) is a well-studied region of massive star formation situated in the Cygnus-X complex (Rygl et al. 2012). Multiple maser emission lines of OH, H_2O and CH_3OH (Araya et al. 2009; Fish et al. 2005, 2011; Kurtz et al. 2004; Kogan & Slysh 1998; Mangum et al. 1992; Plambeck & Menten 1990), indicate the presence of active star formation. In the meantime, the absence of HII regions suggests that the process is currently at an early stage. The region can be resolved into multiple cores (Mangum et al. 1991, Zapata et al. 2012). Two large dust condensations in the region are named MM1 and MM2 and both contain smaller sub-cores, each potentially forming a star. The region has been studied in terms of both continuum dust emission (Mangum et al. 1991, 1992) and molecular lines (Kalenskii & Johansson 2010) and exhibits rich and complex chemical composition.

The research by Minh et al. (2012) is focused on the sub-cores of MM1 (MM1a, MM1b) separately. Their observations were conducted using SMA (Ho et al. 2004). According to their investigations, these sub-cores are regions of massive star formation at the earliest evolutionary stages. Even though being rather close to each

*Email: okochina@inasan.ru

other, the sub-cores manifest themselves differently. The MM1a harbours mostly highly saturated complex organic molecules (COMs), such as CH_3OH, $HCOOCH_3$ and CH_3OCH_3, while MM1b indicates the presence of S-bearing species, such as SO and SO_2. Minh et al. analyzed the data, and estimated the parameters of the cores supposing that the core MM1b should be slightly more evolved than MM1a.

In Van Looveren et al. (2022), we analyzed the story behind the properties of the two sub-cores described in Minh et al. (2012). The study was conducted using the package PRESTALINE (PRESTA + RADEX), a tool that is able to calculate chemical evolution of the object with the given parameters and present it in a form of the line profiles for the selected species (described in the section "The PRESTALINE package"). We adopted some of the assumptions made in Minh et al. (2012), such as temperatures and ages (see the section "Parameters of the objects") and corrected some others, namely, densities (see the subsection "Density and age" in Results) to obtain the observed peculiarities. The main chemical processes shaping the chemical composition of the object were analyzed to explain the origins of the observed differences in spectra (see Results). The key findings of the research conducted are summarized in the "Conclusion" section.

2 The PRESTALINE package

The calculations were carried out with PRESTALINE, a package for modelling and analysing spectral data. The package consists of three parts: PRESTA (Kochina et al. 2013), a one-dimensional model of chemical evolution; RADEX, a radiative transfer code (van der Tak et al. 2007); and a visualisation block (Van Looveren et al. 2021).

To calculate the chemical evolution of a spherically symmetric cloud PRESTA divides the object into concentric cells, with the individually set physical properties. There is neither interaction nor mixing of the cells. The object was also divided into larger units, the regions: an inner one, irradiated by the central source; the outer one, exposed to the background radiation; and the middle dark region.

PRESTA takes into account reactions with cosmic rays (CR), two-body reactions, photoreactions (including the cosmic-ray induced photons), reactions of dissociative recombination with electrons and charged and neutral dust grains, adsorption, desorption, and surface chemistry. PRESTA is able to exploit different sets of initial elemental chemical composition and different chemical networks. For the research presented in this paper, the parameters of both object and the model used for Kochina et al. (2013) were used (see Table 1 for initial elemental chemical composition). The UMIST database (McElroy et al. 2013) was used for gas-phase chemistry. The network contains 582 components and 4524 gas-phase reactions. Surface reactions were adopted from Hasegawa et al. (1992) and Hasegawa & Herbst (1993) but for dimethyl ether and methyl formate synthesis we adopt reactions from Garrod et al. (2008). Reactive desorption was taken to be 5%.

Parameters of a central source needed to reproduce the physical conditions estimated by Minh et al. (2012) in the regions, correspond to massive protostar ($R = 20\,R_\odot$, $T_{\rm eff} = 5000\,$K), as calculated by the radiative transfer code NATALY (Pavlyuchenkov et al. 2012). PRESTA creates files containing the information needed by RADEX for further processing (column densities for the species of interest and

Table 1 Initial component abundances used by PRESTALINE, relative to hydrogen.

Component	Abundance
C	7.3×10^{-5}
N	2.1×10^{-5}
O	1.7×10^{-4}
F	2.0×10^{-8}
He	1.4
Si^+	3.0×10^{-9}
S^+	2.0×10^{-8}
Cl^+	3.0×10^{-9}
Na^+	3.0×10^{-9}
Mg^+	3.0×10^{-9}
Fe^+	3.0×10^{-9}
P^+	3.0×10^{-9}
Dust	2.0×10^{-11}

averaged parameters for every region). The output files of RADEX are then used to calculate the synthetic spectra, as they contain information on a central wavelength, an excitation temperature, and opacity for every transition.

The visualisation block converts the excitation temperatures into Gaussian amplitudes. Possible line overlapping allows us to mix lines and make the synthetic spectra more realistic. Calculations are carried out moving from the inner region to the outer, with the first region being used as the background for the second one. The decrease of the intensity according the opacity of the second region is also taken into account. The same procedure is then repeated for the third layer.

3 Parameters of the objects

The central region of DR21(OH) contains MM1 and MM2, the clumps of comparable size. Minh et al. (2012) confirmed the presence of the sub-structure in one of these clumps: the sub-cores MM1a, MM1b and MM1c. Minh et al. assumed that MM1c was not likely to be an actual core, but the gas heated by the outflow of the neighbour. The mentioned research (Minh et al. (2012)) was focused on the sub-cores MM1a and MM1b. Cores demonstrated curious differences in their chemical composition. MM1a contained COMs (CH_3OH, $HCOOCH_3$, CH_3OCH_3), while MM1b was prominent by emission of the S-bearing species (SO and SO_2). Minh et al. conducted the estimation of the parameters of the sub-cores and came to the conclusion that the core MM1b is further in its process of evolution than its neighbour MM1a (see Table 2).

The parameters used for modelling are presented in Table 3, the difference in density is discussed further. We adopted an age of 10 kyr for MM1a and 40 kyr for MM1b to meet the estimations made in Minh et al. (2012). Physical structure of the objects (see Figure 1) was calculated by NATALY (Pavlyuchenkov et al. 2012). The input parameters for the chemistry were taken from Kochina et al. (2013). Unfortunately, LAMDA database (Schöier et al. 2005), containing the parameters used by RADEX, lacks molecular data for important COMs present in MM1a sub-

Table 2 Parameters of the sub-cores (Minh et al. (2012)).

Parameters	MM1a	MM1b
$n_{\mathrm{H_2}}$ (cm^{-3})	3.5×10^6	2.0×10^6
$N_{\mathrm{H_2}}$ (cm^{-2})	1.3×10^{23}	1.1×10^{23}
T_{core} (K)	200	200
T_{envelope} (K)	20	20
Size ($''\times''$)	$(1.6 \pm 0.3) \times (1.1 \pm 0.2)$	$(1.9 \pm 0.2) \times (1.4 \pm 0.3)$
Age (years)	$< 10^4$	Few $\times 10^4$

Table 3 Parameters of the sub-cores (this work).

Parameters	MM1a	MM1b
n_{H_2} (cm^{-3})	2.0×10^6	4.0×10^6
N_{H_2} (cm^{-2})	1.4×10^{23}	2.4×10^{23}
T_{star} (K)	5000	5000
Size (cm)	4.5×10^{16}	3.8×10^{16}
Age (years)	10^4	4×10^4

core (such as $HCOOCH_3$ and CH_3OCH_3), so within the research we were able to build synthetic line profiles for the limited number of species, concentrating our attention mostly on the S-bearing species, mentioned in Minh et al. (2012), and other simple ones.

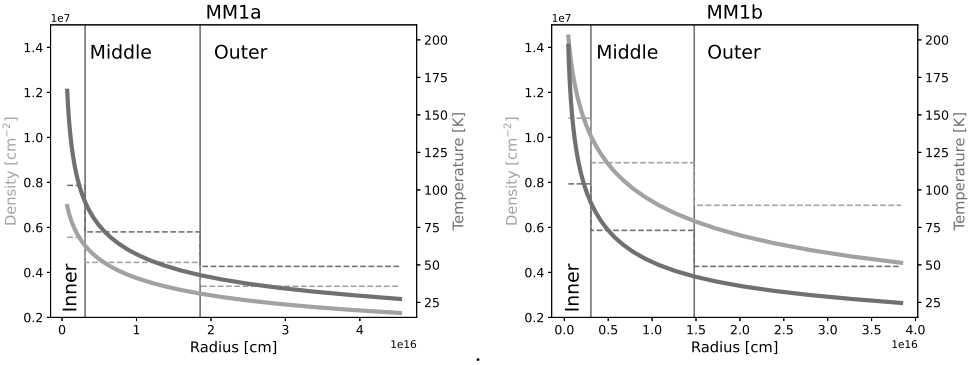


Figure 1 Density and temperature distribution for the models MM1a and MM1b. The profiles were calculated using the radiative transfer code NATALY (Pavlyuchenkov et al. 2012) for the object with the given parameters (see Table 3). Dark grey curves illustrate temperature profiles and light grey – the density ones. The borders of inner, medium and outer regions and averaged parameters used for molecular emission line intensities calculations are marked on the graphs.

4 Results

Figure 2 presents the results of the modelling. The panels clearly show the difference between the cores, described by Minh et al. (2012). By their behaviour the species on the plot can be divided into three groups: sulfur oxides (SO, SO_2), much more prominent in MM1b, the nitrogen-bearing species (CN, CH_3CN, HC_3N, HCN, HNC) more intense in MM1a, and the ones, mostly rather homogeneously distributed within the core, being mostly dependent on the value of the gas density in the object (CO, CF^+, CS).

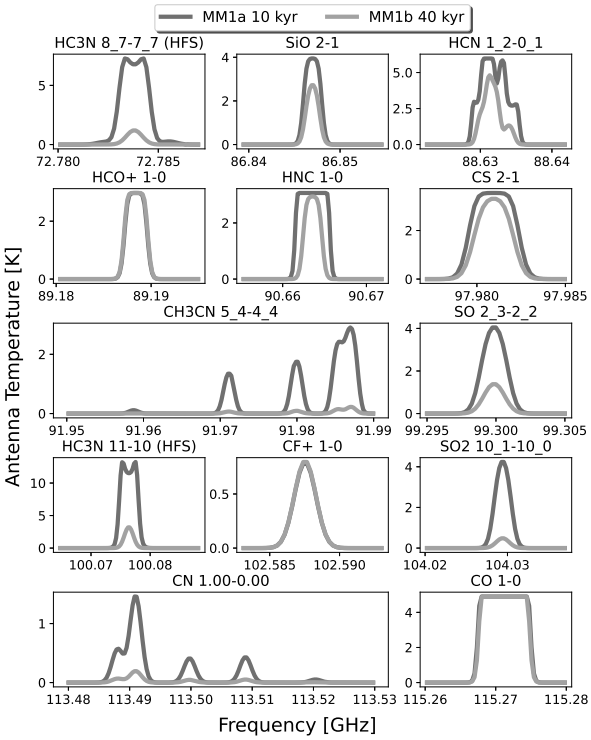


Figure 2 Synthetic comparison spectra, calculated by PRESTALINE, for MM1a and MM1b. Dark grey curves illustrate line profiles for MM1a for the chemical age of 10 kyr and light grey – the ones for MM1b, age 40 kyr. Only one representative transition for each species is shown as the rest follow the same trend.

4.1 S-bearing species

The SO becomes gas due to desorption from the dust grain surfaces, so it mostly originates from the dust. In the inner region of MM1a sulfur oxides are effectively destroyed by the central star's radiation.

$$\mathrm{SO} + UV \rightarrow \mathrm{S} + \mathrm{O}$$

$$\mathrm{SO} + UV \rightarrow \mathrm{SO}^+ + e.$$

In the middle regions CR-induced photons take the role as the destructive factor, not preventing the evaporated species to accumulate in the gas. The second channel of production starts to contribute to the presence of the species in the gas, allowing the line to become visible:

$$SO_2 + UV \rightarrow SO + O.$$

By the edge of the sub-core, destruction takes over again and the abundance of SO decreases. The same trends occur with sulfur dioxide SO_2, the destruction of which is even more prompt and having lower rates of production, it emits even weaker lines.

In MM1b sulfur oxides emit much brighter lines. The column densities of the species within the regions are higher by up to seven orders of magnitude. Being denser in the inner region, MM1b shields SO and SO_2 from the UV field, leading to a different final result even with the same channels of production and destruction. In the middle region evaporation slows down and new leading channels of production there are the reactions of dissociative recombination:

$$HSO^+ + e \rightarrow SO + H$$

$$HSO_2^+ + e \rightarrow SO_2 + H.$$

At the edge of the core destruction rates go higher leading to decrease of the abundance of sulfur oxides.

Another S-bearing molecule, CS, concentrates mostly in the outer regions for both sub-cores and originates from the destruction of more complex molecules (such as H_2CS, C_2S, C_3S, C_4S, H_3CS^+) by CR-induced photons. As the mechanisms and environments there are similar for both clumps, CS abundances are pretty similar for the sub-cores as well.

4.2 N-bearing species

N-bearing species (CH_3CN, CN, HC_3N and HCN) are mostly concentrated in the outer region. Their production is supported by the reactions of dissociative recombination accruing closer to the edge of the cloud and leading to accumulation of the molecules in the outer region.

CH_3CN shows the same trend as the S-bearing species discussed before, where the main destructive agent switches from UV to CR as we move further from the center of the core to the edge.

$$CH_3CN + CR \rightarrow CN + CH_3$$

$$CH_3CN + UV \rightarrow CN + CH_3.$$

Evaporation from the dust, being the main channel of production here is supported by the dissociative recombination:

$$CH_3CNH^+ + e \rightarrow CH_3CN + H.$$

The same happens with HC_3N, but here the supportive reactions are:

$$HC_3NH^+ + e \rightarrow HC_3N + H$$

$$CH_3C_3NH^+ + e \rightarrow HC_3N + CH_3,$$

even becoming the more efficient than evaporation from the grain mantles.

For HCN these are reactions with ions:

$$CH_2CN^+ + e \rightarrow HCN + CH$$

$$NH_2CNH^+ + e \rightarrow HCN + NH_2.$$

At the very edge of the outer region at 10 kyr, the reaction of production with $HCNH^+$ starts to dominate.

$$HCNH^+ + e \rightarrow HCN + H.$$

The same goes for HNC as well.

The behavior of the CN molecule shows the same trend, but unlike the rest, the most supportive reaction for it is the reaction of dissociation of HCN by CR-induced photons:

$$HCN + CR \rightarrow CN + H.$$

MM1a and MM1b share evolutionary pathways of production of N-bearing species, with smaller differences, caused by higher density of MM1b. Still MM1b, being older, expresses an absence of strong CH_3CN, CN and HC_3N lines, caused by general depletion of their main donors, decrease of the abundances of these species, and, consequently, the intensities of their lines.

4.3 Density and age

As it was noticed previously, the study presented here implies the reversed estimations of the density provided in Minh et al. (2012). Adoptation of the values suggested by Minh et al. (2012) (Figure 3) leads to results contradicting the described peculiarities (see Figure 4). So we see the lines of S-bearing species in MM1a spectrum, while MM1b lacks them. Lines of complex organic molecules at the same time become weaker for MM1a. Taking into account the main production and destruction channels

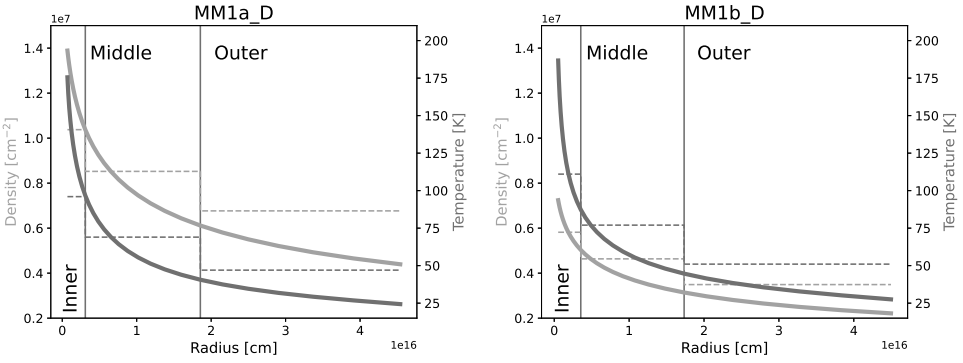


Figure 3 Density and temperature distribution for the models MM1a and MM1b with adopted density values from Minh et al. (2012). The profiles were calculated using the radiative transfer code NATALY (Pavlyuchenkov et al. 2012). Dark grey curves illustrate temperature profiles and light grey – the density ones.

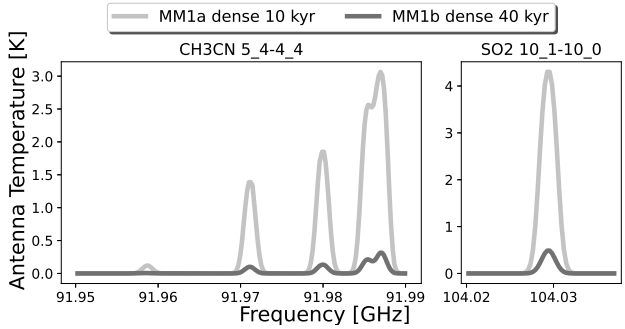


Figure 4 Synthetic comparison spectra, calculated by PRESTALINE, for the models with adopted density values from Minh et al. (2012). Dark grey curves illustrate line profiles for MM1a for the chemical age of 10 kyr and light grey – the ones for MM1b, age 40 kyrs.

of the species discussed above, we suggest that higher density is needed to shield S-bearing species from radiation, keeping their abundance on a detectable level. So we assumed that MM1b core is denser than MM1a.

Unlike the density estimates, we found that the age estimates provided in Minh et al. (2012) are consistent with our results. Their suggestion was MM1a being no older than 10 thousand years and the age of MM1b being few tens of thousands of years. Our implied values are 10 and 40 kyr, correspondingly.

5 Conclusions

In this work we conducted the chemical modelling of the two sub-cores of the well-studied region of star formation DR21(OH). Our goal was to reconstruct and explain the peculiarities in the observed spectra obtained and explained in Minh et al. (2012). We adopted most of the assumptions made in Minh et al. (2012), such as temperatures and ages, but we had to correct the parameter of the density to be able to meet the agreement. According to our estimations, MM1a and MM1b are two protostellar objects at the earliest stage of star formation, with the chemical age of few tens of kyr. MM1b is older, hotter and denser than MM1a.

The analysis of the reaction rates explained the main difference between the sub-cores; and it is the density that is responsible for the observed peculiarities. Most of the explored species show sensitivity to the radiation, be it the one originating from the protostar or the outer field. Denser core provides a better shielding and it leads to difference in the final chemical compound.

The analysis of the reaction rates explained the main difference between the sub-cores; and it is the density that is responsible for the observed peculiarities.

Acknowledgements We would like to express our sincere gratitude to Gwenaël Van Looveren who used to be a member of the PRESTALINE team and provided a great support to the procedures and completion of the presented research.

Funding The studies at Lebedev Physical Institute were supported by the Ministry of Science and Higher Education of the Russian Federation by the grant No. 075-15-2021-597.

References

Araya E.D., Kurtz S., Hofner P. et al. (2009) ApJ 698, 1321
Bottinelli S. , Ceccarelli C., Neri R. et al. (2004) ApJ 617, L69
Fish V. L., Reid M.J., Argon A.L. et al. (2005) ApJS 60, 220
Fish V. L.,Muehlbrad T.C., Pratap P. et al. (2011) ApJ 729, 14
Garrod R.T., Widicus Weaver S. L., Herbst E. (2008) ApJ 682, 283
Hasegawa T.I., Herbst E., Leung C.M. (1992) ApJS 82, 167
Hasegawa T.I., Herbst E. (1993) MNRAS 261, 83
Ho P.T.P., Moran J.M., Lo K.Y. (2004) ApJ 616, L1
Kalenskii S.V., Johansson L.E.B. (2010) Astron. Rep. 54, 295
Kochina O.V., Wiebe D.S., Kalenskii S. V. et al. (2013) Astron. Rep. 57, 818
Kogan L., Slysh V. (1998) ApJ 97, 800
Kurtz S., Hofner P., Alvarez C.V. (2004) ApJS 55, 149
Mangum J.G., Wootten A., Mundy L.G (1991) ApJ 78, 576
Mangum J.G., Wootten A., Mundy L.G (1992) ApJ 388, 467
McElroy D., Walsh C., Markwick A.J. et al. (2013) AAP 550, A36
Minh Y.C., Chen H.-R., Su Y.-N. et al. (2012) JKAS 45, 157
Ospina-Zamudio J., Lefloch B., Ceccarelli C. (2018) AAP 18, A145
Pavlyuchenkov Y.N., Wiebe D.S., Akimkin V. V. et al.(2012) MNRAS 421, 2430
Plambeck R.L., Menten K.M. (1990) ApJ 364, 555
Rygl K.L.J., Brunthaler A., Sanna A. et al. (2012) AAP 539, A79
Schöier F.L., van der Tak F.F.S., van Dishoeck E.F. et al. (2005) AAP 432, 369
van der Tak F.F.S., Black J.H., Schöier F.L. et al. (2007) AAP 468, 627
Van Looveren G., Kochina O., Wiebe D. (2021) Open Astron. 30, 96
Van Looveren G., Kochina O., Wiebe D. et al. (2022) Astron. Lett. 48, 517
Zapata L. A., Loinard L., Su Y.-N. et al. (2012) ApJ 744, 86